Published in final edited form as:
IEEE Trans Biomed Eng. 2007 June ; 54(6 Pt 1): 1016–1030. doi:10.1109/TBME.2007.894629.

A Multi-channel Semicircular Canal Neural Prosthesis Using Electrical Stimulation to Restore 3D Vestibular Sensation

Charles C. Della Santina[1,2], **Americo A. Migliaccio**[1,2], and **Amit H. Patel**[1]

[1]Department of Otolaryngology-Head & Neck Surgery, Johns Hopkins School of Medicine, Baltimore, MD, USA

[2]Department of Biomedical Engineering, Johns Hopkins School of Medicine, Baltimore, MD, USA

Abstract

Bilateral loss of vestibular sensation can be disabling. Those afflicted suffer illusory visual field movement during head movements, chronic disequilibrium and postural instability due to failure of vestibulo-ocular and vestibulo-spinal reflexes. A neural prosthesis that emulates the normal transduction of head rotation by semicircular canals could significantly improve quality of life for these patients. Like the 3 semicircular canals in a normal ear, such a device should at least transduce 3 orthogonal (or linearly separable) components of head rotation into activity on corresponding ampullary branches of the vestibular nerve. We describe the design, circuit performance and *in vivo* application of a head-mounted, semi-implantable multi-channel vestibular prosthesis that encodes head movement in 3 dimensions as pulse-frequency-modulated electrical stimulation of 3 or more ampullary nerves. In chinchillas treated with intratympanic gentamicin to ablate vestibular sensation bilaterally, prosthetic stimuli elicited a partly compensatory angular vestibulo-ocular reflex in multiple planes. Minimizing misalignment between the axis of eye and head rotation, apparently caused by current spread beyond each electrode's targeted nerve branch, emerged as a key challenge. Increasing stimulation selectivity via improvements in electrode design, surgical technique and stimulus protocol will likely be required to restore AVOR function over the full range of normal behavior.

Keywords

vestibular prosthesis; balance; implant; labyrinth; bilateral vestibular deficiency; VOR; vestibulo-ocular reflex; gentamicin; *Chinchilla laniger*

I. INTRODUCTION

Although seldom reaching the level of conscious perception, vestibular sensation – transduction of head rotation, orientation and translation into activity on the vestibular nerves – provides essential input to reflexes that maintain steady vision and posture.[1] When the vestibular nervous system functions normally, the angular vestibulo-ocular reflex (AVOR) stabilizes the eyes with respect to space during head rotations in any direction, using sensory input from the vestibular labyrinths of both ears to generate appropriate control signals for the extraocular muscles attached to each eye. Without this gaze-stabilizing mechanism to keep images still on the retina, visual acuity falls dramatically during head rotations typical of walking, driving and other activities of daily life.[2;3]

Corresponding Author: Charles C. Della Santina, PhD MD, Dept. of Otolaryngology – Head & Neck Surgery, 601 North Caroline St., Room JHOC 6253, Baltimore, MD 21287, voice: 410-955-7381, fax: 410-614-8610, e-mail: charley.dellasantina@jhu.edu.

Normally, head rotation is transduced by a set of 6 semicircular canals (*SCC*), 3 in each ear. Each SCC is a fluid-filled canal that approximates three quarters of a toroid and is attached to the *vestibule* (central chamber of the inner ear) at each end. The fluid within the SCC acts as an inertial load for detection of the component of head rotation about the axis perpendicular to the plane of the SCC. Head rotation generates a moment on the fluid ring within the SCC, causing relative movement between the fluid and SCC walls. This fluid movement deforms the gelatinous membrane (the *cupula*) that blocks the canal lumen within an enlarged bulb at one end of the SCC (the *ampulla*). Just beneath the cupula lies a specialized neurosensory epithelium (the *crista*), within which are hair cells, so named for their bundles of hair-like mechanosensitive stereocilia, which extend from each hair cell into the cupula. Deformation of the cupula causes shear stresses that bend the stereocilia, modulating neurotransmitter release from hair cells and ultimately modulating the nonzero baseline firing rates of afferent nerve fibers that synapse with the hair cells. All axons from one crista coalesce to form an *ampullary nerve* for that crista's SCC, and all axons within one ampullary nerve encode the component head rotation about the corresponding SCC's axis. (Fibers within one ampullary nerve differ in several other important respects, including sensitivity, frequency response, stochastic properties and response to efferent innervation.[4])

The SCCs are arranged across the midline into approximately coplanar, mutually orthogonal pairs: the left and right horizontal SCCs form a *horizontal* pair; the left-anterior [LA] and right-posterior [RP] form a *LARP* pair, and the right-anterior [RA] and left-posterior [LP] SCC form a *RALP* pair. (Due to its anterosuperior location in the labyrinth, the anterior SCC is also commonly referred to as the superior semicircular canal. We will use these terms interchangeably. Similarly, the horizontal SCC is often called the lateral SCC.) Each inner ear's 3 SCCs are arranged to form a (nearly) orthogonal set, so that the pattern of activity on the 3 ampullary nerves of a single inner ear's vestibular labyrinth represent a (nearly) orthogonal decomposition of any head rotation into 3 independent components, each representing the projection of the head rotation's angular velocity vector onto the axis of one SCC.[5] The two SCC comprising a coplanar pair share are arranged in antisense orientation: a leftward head rotation increases firing rates of axons in the ampullary nerve of the left horizontal SCC and decreases the firing rates in the right horizontal SCC's ampullary nerve. Similarly, a head rotation exciting the LA ampullary nerve (a nose-downward, counter-clockwise rotation as viewed from behind) inhibits the RP SCC, and a head rotation exciting the LP ampullary nerve (a nose-upward, counter-clockwise rotation as viewed from behind) inhibits the RA SCC. Differencing and integration of these complementary inputs in the vestibular and oculomotor nuclei of the brainstem generate complementary oculomotor nerve output signals that drive extraocular muscles controlling the angular position and velocity of the eyes with respect to the head. Interestingly, each eye's 6 muscles are arranged in 3 complementary pairs that are approximately coplanar with the corresponding SCC planes, minimizing the neural computational load that would otherwise be required to effectively perform a transformation between coordinate frames of reference. Equally interesting is the vestibular nervous system's ability to perform such transformations when visual and vestibular sensation conflict over more than a few minutes. A subject rotated in the horizontal plane while attempting to visually fixate a scene being moved to simulate a pitch head rotation will subsequently exhibit pitch eye rotations during horizontal head rotation in darkness, an effect called *cross-axis adaptation*.[6;7]

The AVOR acts as an open loop control system via a direct three-neuron reflex arc that does not require moment by moment visual feedback and is thus freed from the ~100 msec delay inherent to visual processing.[8] The AVOR thus works in darkness, and it has a very short latency. In normal humans subjected to passive sinusoidal or transient head rotation in light or darkness over the range of head movements typical of walking, jogging or even vigorous head shaking (>300°/s and >5000°/s^2 over ~0.5–16 Hz), the AVOR gain (conventionally defined

as the absolute value of the ratio of eye and head velocity about the axis of head rotation for sinusoids [or of acceleration for transients]) is near 1 and its latency is only 7–9 ms.[9;10;2;11]. The gain of the AVOR in darkness falls as head rotation frequency decreases below ~0.1 Hz, where vision-dependent tracking mechanisms dominate. In contrast, vision-dependent neural circuits mediating smooth pursuit (reflexive following of images on the retinal foveae) and optokinetic nystagmus (reflexive tracking of the movement of the peripheral visual fields) fail as gaze-stabilizing mechanisms for head movements above ~0.5 Hz and ~50°/s.[12] The AVOR and visual mechanisms are thus complementary, combining to maintain stable gaze across the physiologically relevant range of head movements.

An analogous reflex stabilizing the eyes during head translation (the linear VOR, or *LVOR*) are driven by sensation of linear acceleration, which is mediated by the *utricle* and *saccule* in each ear's vestibule while collectively are called the *otolith endogans*. Each of these sensors transduces translational acceleration of a proofing mass affixed to its *macula*, a neurosensory epithelium analogous to the SCC's cristae except that it is approximately planar and its hair cells are not uniformly oriented. While not entirely flat, the utricular macula lies approximately in a horizontal plane, so utricular nerve axons predominantly carry information about head translational acceleration along directions within the horizontal plane. Similarly, the saccular macula approximates a vertical plane. Departures from planarity for each ensure that the two sensors combined span the range of possible three dimensional translations. In addition to driving the LVOR (which is dominated by the AVOR for far targets but not for visual targets close to the eyes,[13] otolith endorgans provide the essential sensory input to vestibulocolic and vestibulospinal reflexes that stabilize the head and body during standing and walking.

Bilateral loss of vestibular sensation, as can occur after ototoxic drug exposure, infection, trauma or other insults to the inner ear, disables these reflexes and results in illusory movement of the visible world during head motion, postural instability and chronic disequilibrium.[14;15;16] While many victims of bilateral vestibular sensory loss ultimately learn to compensate by enlisting visual and proprioceptive cues to partly supplant missing vestibular sensation, those who fail to compensate suffer significant disability. The lives of these individuals could be significantly improved by an implantable neuroelectronic prosthesis that mimics the normal vestibular labyrinth by measuring head rotation, decomposing it into orthogonal components parallel to the planes of the SCC, and selectively encoding it via electrical stimuli that recreate an appropriate pattern of activity in afferent nerve fibers of the ampullary branches of the vestibular nerve.

Evidence supporting the feasibility of this approach was provided by classic studies of Cohen, Suzuki and their colleagues,[17;18;19;20;21] who described the extraocular muscle activation patterns and direction of conjugate (in SCC coordinates) eye movements in response to electrical stimulation of single and multiple ampullary nerves, corroborating and extending earlier studies of electrical and hydrodynamic stimulation of individual cristae.[22;23;24] Coupled with studies of vestibular nerve afferent responses to galvanic stimuli,[25;26;27] advances in miniaturization of rotational accelerometers, and experience gained from decades of cochlear implant development,[28;29] these studies laid a foundation for development of a head-mounted, implanted prosthesis for emulation of SCC sensation.

Gong and Merfeld described the first single-channel prototype of such a prosthesis.[30;31] In otherwise normal guinea pigs and squirrel monkeys rendered unresponsive to head rotation by surgical plugging of semicircular canals, that device generated partly compensatory eye movements for head rotations about its single axis of rotational sensitivity. Repeated switching of the device between powered and off states revealed progressive reduction in the time required to adapt to each state transition, suggesting that the vestibular nervous system not only adapts to prosthetic input, but learns to do so more quickly with experience.[32] Misalignment

of the prosthesis sensor's axis away from that of the implanted SCC resulted in apparent cross-axis adaptation, suggesting correction of minor misalignments of the device and SCC is within the adaptive range of brainstem neural circuitry mediating the AVOR.[33] Along with these tantalizing results came new challenges. The AVOR gain they observed was significantly less than that of the normal AVOR before canal plugging, suggesting more intense stimuli or more optimal stimulus coupling to the vestibular nerve is needed. In addition, extension of this approach to a multi-channel, multi-electrode device (with assay of eye movement responses in 3 dimensions) is necessary to encode head rotations in all directions.

Unfortunately, the three ampullary and two macular branches of the vestibular nerve are all close to each other in humans[34] and even closer in small research animals.[35] Spurious stimulation of vestibular nerve branches other than the intended target can cause poor control of eye movement direction, corrupting attempts to independently control different ampullary nerves. (Emulation of otolith endorgan transduction represents an even greater challenge, and published attempts have yielded conflicting results, probably due to the close proximity of axons representing different directions within each macule and macular nerve.[36;37;38][39; 40]) Limiting stimulus intensities to those below the threshold of spurious stimulation prevents one from using sufficiently intense stimuli to encode head rotations over more than a small subset of the normal physiologic range. This problem is especially acute for the ampullary nerves of the horizontal and superior cristae, which are especially close to each other and to the utricular nerve. I Extension of the single-channel prosthesis approach to a multi-channel device able to restore normal 3-dimensional AVOR function therefore represents a significant biomedical engineering challenge.

We describe the design, development, circuit performance and *in vivo* testing of a multi-channel vestibular prosthesis that simultaneously encodes head rotations in all 3 dimensions (3D), resolves them into semicircular canal plane components, and presents them as pulse-frequency-modulation encoded stimuli to the ampullary nerves innervating 3 or more SCC. We compare the electrically-evoked AVOR-mediated eye movements in vestibular-deficient chinchillas (*Chinchilla laniger*) to the 3D AVOR of normal animals during head rotation. Finally, we discuss considerations for evolution of this device toward a vestibular prosthesis for treatment of humans disabled by loss of vestibular sensation.

II. METHODS

Adult wild-type 450–650g chinchillas were used for all experiments, which were performed in accordance with a protocol approved by the Johns Hopkins Animal Care and Use Committee.

A. Surgical techniques

To restrain each animal for AVOR testing, a lightweight phenolic post was secured to the skull using dental cement with the animal under isoflurane (3–5% in 4 L/m oxygen) plus local anesthesia (bupivicaine 0.25% and lidocaine 1% with 1:100K epinephrine). The dorsal surfaces of both mastoid bullae were exposed and opened using an otologic drill. A phenolic post was positioned on the skull in the midline and embedded in dental cement (ESPE ProTemp II, 3M Corp, Minneapolis) extruded into each bulla and conforming to the bone surfaces between them to form a rigid connection to skull. The post was oriented so that when the animal was placed into a plastic restraining device within a Fick gimbal mounted atop a servo-controlled rotating table, the plane tangent to the flat part of the dorsal skull (and the occlusal plane of the molars) was pitched 50° 'nose-down' from Earth horizontal. With the animal in this position, the axes of maximal sensitivity of the animal's horizontal SCCs aligned to within ~10° of the Earth-vertical axis of the rotating table. We confirmed this by dissection and direct observation of 3 chinchilla skulls and by subsequent 3D multiplanar reconstruction of micro-computed tomography images of 6 chinchilla skulls,[41] using techniques analogous to those

we have used with human data.[5] (Similar data on 3 chinchilla skulls was reported by others after completion of experiments performed for this study.[42]) In this position, the LA and RP SCC lie approximately parallel to a cardinal *LARP plane* perpendicular to the horizontal SCC and 45° off the midsagittal plane, while the RA and LP SCC lie parallel to a *RALP plane* that is the mirror image of the LARP plane across the midline. (Figure 1) The gimbal could be reoriented so as to bring any of the SCC planes into the Earth-horizontal plane for rotational testing.

To cause bilateral vestibular sensory loss like that humans suffer when injured by aminoglycoside antibiotic ototoxicity, chinchillas were treated bilaterally with 0.5 cc intratympanic injections of 26.7 mg/mL 3 weeks prior to surgery for head post placement and electrode implantation. Gentamicin delivered via this route diffuses to and sequesters within the neuroepithelia of the vestibular labyrinth, where it kills Type I hair cells and causes nearly all Type II hair cells to lose their mechanosensitivity.[43] We[44;45] and others[46] have shown that this results in a marked decrease in AVOR gain for rapid head rotations of direction and sense that normally excites the treated ear's SCCs.

For prosthetic stimulation of ampullary nerves, electrodes were implanted via small windows in the SCC ampullae made using an otologic drill. The anterior and horizontal ampullae were approached via the same opening in the roof of the bullae already prepared for attachment of the post. The posterior ampulla was approached through the posteroinferior chamber of the bulla. Electrodes were fashioned from twisted pairs of 75 um diameter Pt/Ir wire (AS169–40, Cooner Wire, Chatsworth, CA) stripped 0.2 mm, with 0.2–0.3 mm inter-electrode spacing. This spacing was hard to control, as electrodes tended to deform during implantation. Each bipolar electrode pair was directed into one ampulla toward the point at which that ampulla's branch of the vestibular nerve enters its crista, then secured in place with fascia in the ampulla and dental cement in the bulla. For 'monopolar' stimulation via a labyrinthine electrode versus a distant reference, a Pt/Ir wire stripped ~1 cm was embedded in neck musculature. An auxiliary electrode (the eighth electrode, which remained after 3 bipolar pairs were implanted in a labyrinth and 1 reference was placed in the neck) was embedded in neck musculature.

B. Eye movement recording

In preparation for eye movement testing, animals were briefly anesthetized using inhaled isoflurane 3–5% in order to position them in the head restraint within the gimbal. Proparacaine topical anesthetic drops were applied to each eye, and ~0.2 mL bupivicaine 0.25% was injected midway along the expected course of the facial nerve's superior division, to minimize the need for eye lid retraction. Animals were allowed to awaken completely from anesthesia before AVOR testing, as indicated by response to ambient sounds and light touch to the paw or tail.

We employed two methods for eye movement measurement. Three-dimensional video-oculography (3D VOG) was used for sinusoidal head rotations at up to 2Hz, while topically-affixed magnetic search coils were used for higher-frequency sinusoids (up to 15 Hz). While the scleral coil technique [47] is generally considered the 'gold standard' method for measurement of 3D eye rotations, these two methods were complementary. Coil measurements allowed higher (1 kHz) sample rates and finer (0.02°) resolution, and so were especially well-suited for recording small positional amplitude, high-frequency eye rotations. However, our early attempts using surgically implanted coils revealed distortion of eye movements due to surgical trauma and edema. The topically-affixed coils we ultimately used yielded less distortion, but still impacted the eye lids during large amplitude eye rotations that occur during 50°/s head rotations at frequencies at and below ~0.5 Hz. Conversely, our 3D VOG system allowed measurement of larger amplitude eye rotations with less impingement on ocular motion, and allowed direct observation of the eyes during an experiment, but was limited to a relatively low sample rate of 30 frames/sec.

B.1 Video oculography system—The 3D VOG system, which has been described in detail elsewhere,[48] was installed on a Pentium IV 2.4 GHz 1 GB RAM PC running Windows 2000. Firewire cameras (PYRO1394 WebCam, ADS Technologies, USA) retrofitted with ¼" format 16.0 mm focal length, f/2.0 C-mount board lenses (BL160, Allthings Inc., Australia) were used to acquire 640×480 pixel, 8-bit grayscale images at 30 Hz for each eye. An array of 3 fluorescent yellow 0.5 × 0.5 mm squares, separated by 0.5 mm and arranged in a 45° right triangle on a black film, was placed on the topically anesthetized cornea of each eye using a small amount of veterinary tissue glue (VetBond, 3M Corp) after application of proparacaine and saline eye drops. The tissue glue forms a conformal coat over the saline film on the cornea up to the limbus, making a translucent film that remains on the eye and slides under the lids during eye movement, much like a contact lens held by surface tension and suction. A pair of ultraviolet light-emitting diodes (UV LEDs) illuminated each marker, and a UV cut filter on each camera maximized contrast of the markers versus reflections of the LEDs on the conjunctiva. National Instruments LabVIEW 7.0, NI-IMAQ Vision 7.0.1 and NI-IMAQ for IEEE 1394 Cameras 1.5 modules (National Instruments, Austin, TX) were used to control camera settings, threshold the image, correct lens distortion, and determine the center of each marker using a center of mass algorithm. Each eye's center of rotation was achieved by centering a pattern of corneal reflections from LEDs attached to the camera at points equidistant from the lens axis. The initial and instantaneous pixel positions of each marker were used to construct a rotation matrix representing the instantaneous 3D angular position of the eye, from which Euler angles, rotation vectors and quaternions were calculated.[49;50;51] The resolution of the VOG system was < 0.2° (limited by image pixelization) and the velocity noise was < 3°/s RMS (<5°/s peak) in each dimension. While a 30 Hz sample rate ideally allows recovery of signal components at up to the Nyquist rate of 15 Hz, we found in practice that amid quantization noise, about 8–10 points per cycle of an approximately sinusoidal response were required to give a clear indication of the cycle by cycle response as we monitored it in real time. We therefore limited the use of 30 Hz VOG to measurement of eye movements up to 2Hz for these experiments, complementing VOG data with coils data at higher frequencies.

B.2 Magnetic coil oculography system—Adapted from the scleral coil technique originally described by Robinson [47] and modified to use topically affixed coils as previously described by others,[52;53] our coil system and technique been described in detail elsewhere. [49;50] Three pairs of field-generating coils were rigidly attached to a superstructure that moved with the animal. The three magnetic fields were mutually orthogonal and aligned with the X (anterior-posterior), Y (interaural) and Z (superior-inferior) coordinate axes. The X, Y and Z fields oscillated at 83.3 kHz, 55.5 kHz and 41.6 kHz, respectively. On each eye, two insulated copper watch coils (2 mm diam, 80 turns, ~3 mg each) were glued orthogonal to one another with cyanoacrylate, then affixed to the surface of the topically anesthetized eye as described above. The mass of the coil assembly is ~20 mg, and its center of mass sits ~1.5 mm from the surface of the eye. Lead wires to recording equipment were strain-relieved, suspended parallel to the motor axis, and tightly twisted to minimize movement artifacts generated by loops within the magnetic fields. Lead connectors were kept fixed with respect to fields during calibration and during the experiment. Applied duction of the coils under microscopy in anesthetized animals before and after testing sessions confirmed absence of slippage with respect to the eye. Each coil pair remained in place for about 30–60 minutes (depending mainly on whether large-amplitude eye movements caused the coils to impact the eye lids) before precipitously losing adherence to the eye, an event accompanied by a sudden and obvious drop in apparent eye movement. Whereas this topical technique yielded AVOR gains similar to those measured using VOG at midrange frequencies, our initial series of experiments using coils sutured to the sclera beneath conjunctival flaps yielded much lower apparent AVOR gains, suggesting mechanical restriction of eye rotation by edema or impact of sutured coils on orbit contents.

A full description of the calibration and signal processing methods applied to these signals has been described elsewhere.[54] Currents from each eye coil were demodulated to produce three voltages proportional to the angles between each coil and each magnetic field, then passed through 8-pole analog Butterworth anti-aliasing filters with a corner frequency of 100 Hz. Coil signals were digitized at 16-bit resolution at a sampling rate of 1 kHz. The noise-equivalent input of the system was equivalent to a peak-to-peak eye position deviation of 0.02°.

C. Mechanical Rotation Stimuli

The gimbal structure holding the animal mounted on a servo-controlled motor (model 130–80/ACT2000; Acutronic USA, Inc, Pittsburgh, Pa) positioned so that the center of the animal's skull was aligned with the rotator's Earth-vertical axis. The gimbal was reoriented to bring each axis of interest coincident with the rotator's axis for each of 3 axes: horizontal (yaw), left-anterior/right-posterior (LARP, left ear down nose up) and right-anterior/left-posterior (RALP, right ear down nose up). The horizontal AVOR was tested with the gimbal in its reference position, in which the animal's horizontal semicircular canal axes were approximately Earth-vertical. The LARP and RALP axes were approximated as being 45° off the midline and in the plane of the horizontal semicircular canals. LabVIEW-based software controlled presentation of sinusoidal and transient rotations. Sinusoids included rotations at 0.05–15 Hz at peak velocity 50°/s. Stimulus duration was sufficient to include at least 6 cycles at each frequency, and only cycles not corrupted by blinks or other artifacts were analyzed.

D. Electrical Stimuli

Functional electrical stimulation experiments were initially performed using a rack-mounted apparatus for identification of effective stimulus parameters. Either a function generator (for electrical-only trials) or a signal encoding the instantaneous angular velocity of the rotator (for simulation of the prosthesis during head rotation) was used to modulate the pulse frequency of constant-current, charge-balanced biphasic pulses from a set of rack-mounted stimulators (AM 2100, AM Systems, Carlsborg, WA). Electrical stimuli were delivered via pairs of electrodes in 'bipolar' (both electrodes in the ampulla) or 'monopolar' (one in the ampulla, one in the neck) format, with the former typically requiring higher currents to achieve a response but exhibiting slightly better selectivity. Each biphasic pulse was defined by 4 Intervals: (Interval 1) a constant-current pulse cathodic on the 'active' electrode nearest the nerve, typically 20–400 μA and 20–500 μs; (Interval 2) a no-current 'intra-pulse interval,' typically set to 10% of duration of Interval 1; (Interval 3) a charge-balancing pulse equal and opposite that of Interval 1; and (Interval 4) a zero-current interval of duration dynamically adjusted to achieve pulse-frequency-modulation over a range of 30–300 pulse/s. Once approximately optimal stimulus parameters were determined for each pair of electrodes, those parameters were encoded into the firmware of the head-mounted prosthesis for subsequent experiments.

E. Data Analysis

A software suite developed by one of the coauthors (AAM) was used for analysis of 3D eye movement data from coil and video oculography. All data are preprocessed by modules specific to the technology used for data acquisition, then analyzed as rotation vectors with roll, pitch and yaw components in the right-handed head coordinate system shown in Figure 1. Velocity vectors were calculated from the corresponding rotation vectors, then filtered using a low pass filter (50-order, zero phase, finite-impulse-response, f_o= 40 Hz) or a running spline interpolation filter (LabVIEW 'Cubic Spline Fit' module with balance parameter 0.99995) applied to data linearly interpolated to a 1 kHz time base. For eye responses to sinusoidal stimuli, each of the three eye movement components (horizontal, LARP and RALP) was separately averaged cycle-by-cycle for least 5 cycles free of saccades, blinks or evidence of

distortion due to marker or coil slippage or lid impact. Variation about each average eye movement cycle waveform is reported as ±1 standard deviation about the mean waveform, computed individually for each point. For each axis about which head rotations were presented, AVOR gain was defined as the ratio of peak eye and head velocity for the component about that axis. AVOR phase was defined so that a positive phase lead meant that the eye movement velocity led the ideal eye movement (which is equal in magnitude and 3D direction but opposite in sense from the head rotation).

III. 3D Multi-channel Vestibular Prosthesis

As illustrated in Figure 2, the multi-channel vestibular prosthesis is designed to simultaneously encode head rotation in each of 3 dimensions and deliver pulse-frequency-modulated, biphasic, constant current stimuli via pairs of up to 8 electrodes. It comprises a microcontroller that continually samples input from 3 mutually orthogonal angular rate sensors and accordingly modulates the pulse frequency of stimuli delivered by a shared current source switched between pairs of electrodes. Any combination of 'bipolar' (two electrodes are both within a given ampulla) and 'monopolar' (one electrode in the ampulla, the other in neck musculature) electrodes can be configured post-implantation under software control, resulting in up to 4 isolated bipolar electrode pairs or up to 7 monopolar electrodes with a common reference. The following sections describe the device in more detail.

A. Sensors

The 3 micromachined gyro angular rate sensors (ADXRS300, Analog Devices, Norwood, MA) are oriented orthogonal to each other. Each encodes rotational velocity about a single axis at a resolution of ~0.2°/s (least significant bit after digitization) over a range of −450 to +450°/s with bandwidth of DC-40 Hz. The device is affixed to the head post in an orientation that approximately aligns (to within ~10°) the sensors with the planes of the implanted SCCs, so the output of each sensor can directly modulate the pulse frequency of the corresponding SCC's electrodes. These devices were chosen because of their small size (7×7×3 mm); sensitivity range, noise and bandwidth well matched to the physiologic system; and commercial availability. Their main disadvantage is high power consumption (30 mW continuous for each gyro), which accounts for 90% of the consumption of the prosthesis. A second disadvantage is the need to mount them with the 7 mm dimensions in the plane of rotational sensitivity, which places a constraint on how thin the device can be in a future version for subcutaneous implantation in humans.

B. Processor

An MSP430F149 microcontroller (Texas Instruments, Dallas, TX) clocked by a 6 MHz crystal controls the device, sampling gyro signals and generating pulse-frequency-modulated biphasic current pulses of user-controllable level and duration on electrodes in the corresponding SCC's. Apart from its ultra-low power consumption, several features of this device make it advantageous for our application. Well-supported by simple but powerful debugging software, this device incorporates several of the circuit modules needed for our design in a single 10×10×1.8 mm package, including a 16-bit central processing unit (CPU), 16 bit hardware multiplier, 2 KB of RAM, 60 KB of flash memory, two multifunction timers, an 8-channel 12-bit analog-to-digital converter (ADC), and a JTAG interface that allows *in situ* reprogramming of the prosthesis via a 6-wire interface.

While a less powerful microcontroller with fewer integrated modules could have met our current design's criteria, we chose the MSP430F149 because it exceeds those criteria in ways that leave room for enhancements to the existing design. For example, the CPU and hardware multiplier can perform a 3 × 3 rotation matrix multiplication of the 3 × 1 input data vectors at

the 100 Hz rate with which the prosthesis samples gyro inputs, which may prove necessary to correct for gyro/SCC misalignment if central nervous system adaptation alone proves inadequate. The ADC's unused inputs can support addition of a 3-axis linear accelerometer to emulate utricular and saccular sensation, a circuit for monitoring electrode impedances, and measurement of electrophysiologic responses to brief electrical stimuli. A 3-wire RS-232 serial interface module can support a simple user interface administered by the microcontroller CPU, as might be needed to allow a clinician or implanted patient to adjust device parameters.

C. Current Source and Switching

One current source is shared by all channels of the device. It is a single-supply voltage-to-current converter built around an op-amp (OPA2345, Texas Instruments) chosen for its low power consumption and adequately high slew rate (2 V/μs). The op amp output sets the gate voltage of an enhancement-mode N-channel field-effect transistor as required to maintain a current of 0–512 μA through one pair of electrodes and a 3 KΩ sense resistor The current is set for each channel by one of the 3 channels of an 8 bit digital-to-analog converter (MAX 5101, Maxim, Sunnyvale, CA) under CPU control, yielding 2 μA resolution.

Each of 8 electrode leads connects via a 1 μF capacitor to one of 8 normally open outputs of each of 2 analog multiplexers (MAX308, Maxim). The common pin of the "anode side" MAX308 connects to a 24 V compliance voltage generated by a step-up converter (chosen to allow >2 mA via a 10 kΩ combined electrode impedance, or >200 μA through 100 kΩ), while "cathode side" MAX308 common terminal connects to the current source. Stimulation via a given pair of electrodes Z1 and Z2 consists of 4 intervals. During Interval 1 (the 'active phase' of a 'biphasic pulse', typically 200 uS), the microcontroller commands the MAX308's to connect Z1 (initially the anode) to 24 V and Z2 (initially the cathode) to the current source. During Interval 2 (the 'intra-pulse interval', typically 40 uS), both MAX308's are disabled, disconnecting both electrodes. During Interval 3 (the 'charge-balancing phase', typically 200 uS), commands for the two MAX308's are swapped to make Z1 the cathode and Z2 the anode. During Interval 4 (the 'interpulse' interval), both electrodes are again disconnected, this time for a duration equal to the inverse of the pulse rate, which is modulated according to the most recent sample of input from the corresponding gyro.

The essential parameter defining the "intensity" of a biphasic stimulus pulse is the charge withdrawn from (at the active, cathodic electrode) or injected into (at the reference electrode) the surrounding tissue during the excitatory phase of the biphasic, charge-balanced pulse. [55] To control the amount of charge injected, one may control the pulse current, the pulse duration, or both. Which one is altered does not matter, as long as the total charge injected remains within the window for "safe stimulation" for a given electrode (beyond which irreversible electrochemical reactions corrode the electrode and may poison adjoining tissue [56]) and commanded current does not exceed the ratio of the stimulator's compliance voltage and the electrode impedance. In our present experiments, we typically set the pulse current for Intervals 1 and 3 equal (but opposite) at 50–400 μA, depending on the responses observed. We typically leave the duration of pulse intervals 1 and 3 at 200μs, although this can be changed on the fly with 0.16 μs resolution by the 6 MHz timer.

We have only used symmetric rectangular pulses (constant equal current and equal duration for Intervals 1 and 3), with head angular velocity modulating pulse rate but not pulse shape or charge per phase. However, the circuitry can generate pulses of arbitrary shape (subject to charge-balancing requirements and the D/A converter's 8-bit resolution, 6 uS settling time and 0.6 V/uS slew rate), such as 'pseudomonopolar charge-balanced pulses' (brief, high current cathodic phase followed by a longer duration, lower current anodic phase), which may be more potent for the given amount of charge passed.[57]

D. Power

Uninterrupted power is important for this application, because an implant recipient adapted to tonic stimulation could suffer severe vertigo due to sudden cessation of prosthetic vestibular input. A lithium battery contained within the head-mounted device package (Saft LS14250, 3.6 V, 1000mAh, 14.7mm diam × 24.8mm, 8.9g) can act as a backup for a rechargeable battery contained within a body-worn pack (Lenmar LIJ408, 7.2 V, 1100mAh, 54×38×22mm, 71g), simplifying replacement of batteries without interruption of power delivery. Unfortunately, the high current draw of the 3 gyros limits battery life to about 48 hours per rechargeable battery. The MSP430 and low-level logic devices draw comparatively negligible current from a second regulator generating a 3 V supply. Finally, an inductor-based step-up DC-DC converter generates the 24V compliance voltage for the current source, which draws negligible mean power due to the low amplitude and duty cycle of stimuli.

E. Software

We use the Kickstart Embedded Workbench (IAR Systems, Foster City, CA) and FET430 flash emulation tool (Texas Instruments) for program development and flashing the microcontroller's memory via its JTAG interface. This powerful interface also allows one to monitor and change register and memory values as the device is running in situ.

After initializing stimulus parameters and conveying current level commands to the D/A converter, the MSP430F149 reverts to a low power mode. From that point, the software's action is organized around three interrupt service routines that control the timing of gyro sampling, pulse frequency modulation (Interval 4), and fine resolution of biphasic pulses (Intervals 1–3).

One interrupt service routine triggered every 10 ms by a slow (32768 Hz clock crystal) timer samples all three gyro inputs (at 100 samples/S) and accordingly sets the Interval 4 duration for each stimulus channel. It also polls a set of memory locations that can be changed via the JTAG interface without disturbing the microcontroller, providing a simple command interface for adjusting stimulus parameters while the device is running.

A second interrupt service routine is called whenever one of three timers (one per gyro) signals the end of Interval 4 for that gyro's channel. This routine resets that timer according to the most recent input from that gyro, then checks to see whether the current source is already in use by another channel. If so, the new channel's request is queued for later. Otherwise, the routine connects the appropriate electrode pair to initiate Interval 1, signals that it now owns the current source, and sets a 6 MHz timer to later announce the completion of Interval 1.

A third interrupt service routine, which is triggered upon completion of Intervals 1, 2 and 3, checks which interval is ending and sets the current source connections appropriately for the next interval. If Interval 3 is ending (signifying the end of a biphasic pulse on the presently active channel), the routine activates a pulse on the next channel in the queue. The queue is rarely > 1 element long, because the relatively low pulse rates (<350 pulses/S on each of 3 channels), low probability of a maximal pulse rate occurring simultaneously on all the three channels, and the brevity of pulses result in a low rate of clashes between two channels simultaneously demanding access to the current source.

For each channel, the interval Δ determining the instantaneous pulse rate is computed from the 12-bit ADC output x_i representing head velocity (ADC values of 0, 2048 and 4095 representing gyro velocity −450, 0 and +450°/s, respectively) by interpolation into a parameterized look up table, with values described by

$$f = 0.5 \times f_{max} \times (1 + \tanh(A + C(\frac{x_i}{2048} - 1))$$
$$\Delta T = 1/f$$
$$A = \tanh^{-1}(2 \times f_{baseline}/f_{max} - 1) \quad (1)$$

where f is the pulse rate in pulse/S, x_i = [0..4095] is the ADC input, $f_{baseline}$ is the pulse rate for zero head velocity (typically set to 100 pulse/S), f_{max} is peak pulse rate (typically 350 pulse/S), and C (typically set to 5) is a compression factor that determines the slope of the pulse rate versus head velocity curve around the baseline rate. As illustrated in Figure 3, this function describes a saturating nonlinearity that roughly emulates the spike rate versus head velocity operating curve of regular chinchilla vestibular nerve fibers,[58] up-shifted to a resting rate of 100 pulses/s when the head is at rest to allow the device to overdrive spontaneous afferent fiber activity and thus provide more dynamic range for encoding inhibitory head rotations. Multiple pulse rate versus velocity mappings parameterized via different combinations of C, f_{max} and $f_{baseline}$ can be stored within the microcontroller's flash memory. Prior to this calculation of pulse modulation timing, each input data stream can pass through a digital high pass filter emulating the characteristics of the chinchilla semicircular canals, like that described by Gong and Merfeld.[30] Stimulus amplitude and pulse shape can be modulated by head angular velocity or acceleration with a similar approach.

F. Packaging and Mounting

Figure 4 shows a photograph of the prosthesis circuitry prior to packaging. The circuitry is implemented using surface mount technology and is ~30×30×11 mm; when packaged within a 35×35×15 mm plastic case, it weighs 19g without the battery. While approaching the size of cochlear implants in clinical use, this is still too large to fully implant within a chinchilla, so we mount the case to the skull extracranially and connect to implanted labyrinthine electrodes via a percutaneous connector. An angled coupler rigidly holds the case on the phenolic head post so that the axis of maximal sensitivity of each gyro aligns to within ~5° with the cardinal horizontal, LARP or RALP axis corresponding to the SCC it emulates.

F. Circuit Performance

Figure 5A shows the frequency of output pulses on each of three channels configured for biphasic stimulation of the horizontal, anterior and posterior semicircular canals of one vestibular labyrinth during 2 Hz, 50°/s rotation about each SCC's axis. While imperfect alignment of the device with the motor axis led to some crosstalk (e.g., modulation on the horizontal channel during RALP axis rotation is 8% of the RALP modulation), the device's ability to encode 3D rotations is apparent. Figure 5B shows the stimulus current delivered via one pair of electrodes during 240 μA/phase pulses of 50, 120 and 200 μs/phase, with cathodic-to-anodic intrapulse interval set to 10% of the duration of each phase as measured across a 100 kΩ resistor in series with electrodes immersed in 0.9% NaCl in water. With 3 channels running continuously at 100 pulse/s baseline rate delivering 200 μA/phase, 200 μs/phase pulses on 3 channels across electrodes in saline, the device drew a mean supply current of 19.1 mA from a 7V source.

III. RESULTS

A. 3D AVOR in Normal Chinchillas

To establish criteria against which to judge effects of prosthetic stimulation in subsequent experiments, we first examined the AVOR of 5 normal chinchillas. Figure 6, column 1, shows all canal plane components of mean eye velocity for each eye during 2 Hz, 50°/s head rotations of a normal chinchilla in the horizontal, LARP, and RALP directions. The number of

overlapped and averaged cycles is listed for each panel. The standard deviation for every point in time for every trace was < 5°/s, so traces representing ±1SD are not shown to avoid obscuring mean traces. Averaged over all normal animals, the mean ±1SD gain and phase lead (expressed as a lead versus the ideal eye response of −1 times the head velocity) during 2 Hz, 50°/s head rotations were (gain 0.43±0.28, phase 2.7±11.2°) in the horizontal plane; (0.48±0.1 and −2.0 ±7.3°) for LARP; and (0.45±0.09 and −4.2±8.4°) for RALP. Traces representing these mean normal responses are shown in each panel of Figure 6 for comparison to individual animal responses. Figure 7 shows the gain and phase of the horizontal component of the AVOR during sinusoidal horizontal head rotations at 50°/s peak velocity and 0.05–15 Hz, pooled for measurements in the 5 normal animals. These data are consistent with published data for the 1-dimensional horizontal AVOR in normal chinchillas.[59].

Several features of the normal chinchilla 3D AVOR are apparent. Both eyes move with approximately equal speed and direction about an axis approximately aligned with the axis of head rotation. Responses are approximately symmetric about each rotation axis. The AVOR partially stabilizes the eye with respect to space for head rotations from ~0.2–10 Hz. The gain decreases for frequencies below ~0.1–0.2 Hz. The AVOR phase lead is small over ~0.5–10 Hz but increases with decreasing frequency below ~0.2–0.5 Hz, typical of a high pass filter with a break frequency at ~0.05–0.1 Hz. There is a trend toward a slight phase lag at 10–15 Hz; however, the lag is smaller than one would expect from the 12–14 ms latency of the normal chinchilla AVOR response to transient head rotations. This is consistent with the phase lead observed in recordings from vestibular nerve afferent fibers and attributed to the dynamics of action potential initiation [58;60]

B. 3D AVOR of Chinchillas with Bilateral Vestibular Deficiency Due to Gentamicin

B.1 Responses to Head Rotation Alone—In 3 chinchillas treated 3 weeks earlier with bilateral intratympanic administration of gentamicin, implanted with electrodes in the 3 SCC's of the left labyrinth, and then allowed to fully awaken before testing, only minimal (<2°/s RMS) AVOR-mediated eye movements were observed during head rotations in any direction when presented without prosthetic stimulation. Figure 6, Column2 shows the mean responses of one such animal (ch050506B) during 2Hz, 50°/s head rotations about each SCC axis in the absence of vision. The other two yielded similar results. Across all frequencies, eye velocities were small enough that a response at the stimulus frequency could not be discerned above the noise floor of our recording system.

B.2. Responses to Head Rotation with Prosthetic Electrical Stimulation—Each of the implanted, vestibular-deficient chinchillas was then retested with prosthetic electrical stimuli modulated by head rotational velocity. Figure 8 shows the horizontal components of left and right eye rotational velocity for ch050506B), during continuous 2 Hz 50°/s peak sinusoidal horizontal head rotations without and then with prosthetic electrical stimulation. For this trial, only the left horizontal SCC electrodes were activated; the LA and LP electrodes were kept off to help isolate the effect of LH stimulation. Stimulus parameters were: cathodic-first biphasic pulses via a bipolar electrode pair in the left horizontal SCC ampulla, 200 μA/phase, 200 μs/phase, modulated with sigmoid defined by Equation 1 with f_{peak} 300 pulse/s, $f_{baseline}$ 100, C=5. Before electrical stimulation begins (Panel A, up to t=55 sec), head rotation elicits no AVOR. When electrical stimulation encoding head velocity begins (Panel A, ~t=55.7 sec), brisk, asymmetric horizontal eye movements occur, with rightward (negative) peak slow phase nystagmus velocities nearly equal to peak head velocity and small compensatory leftward quick phases, consistent with excitation asymmetry due to stimulation of only the left ear. Adaptation to this purely unilateral electrical stimulation was remarkably quick. Panel B is a segment of the same trial as Panel A, less than 20 sec after onset of prosthetic stimulation. The slow phase nystagmus is already more symmetric in direction, tracking horizontal head velocity

with a mean gain for the two eyes very similar to the normal animals' mean gain of 0.43. There is some disparity between the left and right eyes' responses (which, although not consistently observed across animals, might indicate an LVOR contribution via spurious stimulation of the macular nerves, assuming eye movements evoked purely by ampullary nerve stimulation are conjugate[21]), the 1-dimensional responses in Figure 8AB suggest a prosthetically-evoked horizontal AVOR that is close to normal in 1D. However, 3D analysis reveals that the evoked eye movements have significant LARP and RALP components instead of the purely horizontal movement desired. Figure 8C, which shows the mean±1SD cycle-by-cycle average for all eye velocity components for both eyes over the 17 cycles beginning at t=67 of the trial shown in 8B, demonstrates that while the horizontal components are close to the normal response gain, the LARP components are comparable in amplitude with the desired horizontal response, with the eyes making an upward and clockwise (from the animal's viewpoint) rotation about the LARP axis when they are moving to the right about the horizontal axis during the second half of the cycle, when pulse rates are maximal. This is consistent with simultaneous excitation of the closely apposed ampullary nerves to the left horizontal (intended target) and LA (bystander) ampullary nerves. During the same phase of the stimulus, there is also a smaller component about the RALP axis; however, its sense (upward and counter clockwise in the second half of the cycle) is opposite the expected effect of LP ampullary nerve excitation, and therefore suggests otolith excitation. When the same data are considered in cardinal X,Y,Z head coordinates, it is clear that the two eyes are moving about two different axes. The left eye (ipsilateral to the site of stimulation) is yawing rightward and pitching upward during peak stimulation with a small clockwise roll. The right eye is also yawing right and pitching up, but it exhibits a much more prominent clockwise roll. Upward and clockwise, disconjugate eye rotations with left stimulation are typical of all responses Curthoys reported for selective stimulation of the utricle or saccule.[36]

Subsequent activation of the remaining channels of the prosthesis (with stimulus parameters optimized individually for each electrode channel) caused a brisk nystagmus beating counterclockwise and leftward, which adapted down to a slow phase velocity of <5°/s in all components within 20 minutes. Figure 6, Column 3, shows all components of the mean AVOR responses for ch050506B during 50°/s peak sinusoidal horizontal, LARP and RALP head rotations at 2 Hz with the prosthesis active, after 3.5 hours of prosthetic stimulation. At this point, electrodes in the LH, LA and LP SCC were all continuously delivering 100 pulses/sec even with the head still, and each modulated with head rotation parallel to the appropriate implanted left labyrinth SCC. While the prosthetically-restored AVOR is less than at onset and exhibits some cross-axis components and departures from conjugacy suggesting spurious stimulation, all directions of head rotation yield eye movements clearly closer to normal with prosthetic support than without it (compare Column 2). Responses to 2Hz 50°/s LARP and RALP plane rotations (middle and lower panels of Column 3, respectively) are similar.

Columns 4 and 5 of Figure 6 show responses for the two other gentamicin-treated animals tested under analogous conditions after 5 days (ch072106) and 3 days (ch071405) of prosthesis use. Neither animal had any measurable response to head rotation without prosthetic input, so those results (which look like Column 2) are not shown. For head rotation with prosthetic stimulation, each animal exhibited responses in one or more SCC planes that were closer to normal than without prosthetic stimulation, but often with spurious components indicating current spread beyond the targeted SCC's ampullary nerve. Chinchilla ch072106 exhibited especially prominent responses to LA and LP excitation, with the slow-phase nystagmus during the peak of stimulus pulse frequency more than double the mean eye velocity for normal chinchillas' responses. Unfortunately, the LH electrode was not well secured in this animal, and responses to horizontal head rotation were therefore small. The long-term time course and ultimate extent of adaptation to continuous prosthetic use will be the topic of future study.

The frequency response for prosthetic stimulation encoding horizontal head rotation averaged across all 3 animals is compared to the normal animals' responses in Figure 7. Although variability prevents drawing strong inferences about the underlying dynamics, the prosthetic response curve is steeper and has no clear inflection around 0.05–0.1 Hz, the slope of log(gain)/log(frequency) is close to ½, and there appears to be a shift toward greater phase lead that normal across the frequency range tested. (No prefiltering of gyro signals like that in [30] was implemented for these experiments.) Taken together, these features are reminiscent of the fractional zero Laplace operator characteristics commonly used to describe the dynamics contributed by vestibular nerve afferents' spike initiation mechanisms.[61;60] Interestingly, the upward slope of the magnitude curve seems to most closely approximate the dynamics of vestibular nerve afferents with irregular spontaneous discharge, which are much more sensitive to exogenous electrical currents applied via implanted electrodes than are fibers with regular spontaneous activity.[25]

The growth of both the desired response and spurious components due to current spread is illustrated by Figure 9, which shows all eye movement components during a 2 Hz, 50°/s RALP head rotation encoded by prosthetic stimulation delivered by a monopolar electrode implanted in the left posterior SCC ampulla with respect to a distant reference in ch050506. In this case, stimulus current was varied from 50 to 250 μA, with all other parameters kept constant ($f_{baseline}$ = 100, f_{peak} = 350, C = 5, 200 us/phase, cathodic first). In each panel, the ordinate axis and head velocity trace have been scaled to enhance visibility all components of the response. The RALP component of the response (which is appropriate for the stimulus) is barely detectable at 50 μA. At 100 μA, the eyes are making a conjugate, appropriately directed rotation similar to that observed in normal chinchillas, except for a horizontal component that could indicate horizontal SCC ampulla or otolith nerve stimulation. At 250 μA, the LP response has grown to over 150°/s peak velocity; however, the horizontal component also grows with increasing current amplitude, equaling the RALP response in amplitude at a stimulus current of 250 μA.

C. Postural Behavior of Vestibular-Deficient Chinchillas During Prosthetic Stimulation

While we did not quantitatively measure postural and gait changes due to ototoxic injury and prosthetic stimulation, we did observe qualitative behavioral responses consistent with the expected effects of each manipulation on activity of each labyrinth. Unilateral intratympanic treatment with gentamicin typically causes stereotyped pattern of postural effects starting about 7–10 days after injection.[44;43] These include (for a left injection) a left-ear-down combined roll/yaw head tilt and extension/abduction of the right forelimb. This usually resolves over the subsequent 4–5 weeks, as the animal compensates for the stable reduction in vestibular sensation from the treated ear. Following bilateral intratympanic gentamicin administration, our animals developed postural and behavioral signs consistent with a transient asymmetry of vestibular sensation, including a head tilt and contralateral limb extension/abduction, consistent with one ear leading the other in development of gentamicin-induced injury. Once these acute changes resolved (suggesting equivalent damage to both labyrinths), animals exhibited unsteady gait and tendency to run rapidly in circles when startled. Implantation of electrodes in the left labyrinth caused an additional left ear down head tilt in one bilaterally gentamicin-treated animal, suggesting further decrement from a nonzero level of spontaneous vestibular afferent activity in the implanted labyrinth. The other gentamicin-treated animals exhibited no sign of additional injury due to implantation.

Chinchillas responded to commencement of left labyrinthine prosthetic stimulation with postural reflexes typical of acute relative right hypofunction, including a rightward and clockwise (from the animal's perspective) head rotation to a stable position of right-ear-down head tilt. The head tilt persisted but reduced gradually over subsequent days, and was absent

(per visual inspection of the unrestrained animal) after 2 days of continual prosthesis use. Brief power outages that accompanied battery changes then caused a leftward and counter-clockwise head rotation, which ceased with restoration of power from the new battery. This is consistent with vestibular central nervous system compensation to a new stable point, from which transient cessation of left labyrinth prosthetic stimulation is interpreted as acute onset left vestibular hypofunction.

IV. DISCUSSION

To restore the 3D AVOR, a vestibular prosthesis should encode 3 separable components of head rotation and emulate normal sensory transduction on at least 3 ampullary nerves. Although simultaneous restoration of normal AVOR for all 3 SCC in a single animal remains an elusive goal, we have demonstrated *in vivo* the first multichannel head-mounted vestibular prosthesis capable of meeting this challenge.

As illustrated by Figure 9, stimulus selectivity is a key determinant of performance, because poor selectivity causes retinal image slip when stimuli are of intensity sufficient to encode full range of head rotation velocities and accelerations for which the AVOR is most important. Anatomically-guided design and placement of electrodes, like the approach successfully used with cochlear implants,[62;63] could help bring electrodes closer to target ampullary nerves while shielding other nerves nearby. Judging from the spectral selectivity achieved by cochlear implants, increased vestibular nerve stimulation selectivity should be achievable through such refinements in electrode design. Optimization in stimulus protocols and surgical technique could improve outcomes further. The selectivity problem is likely less severe in humans than in chinchillas, due to significant difference in separation between vestibular nerve branches.

Several additional hurdles remain prior to application of this technology to humans disabled by vestibular sensory failure. Like cochlear implants currently in use, a vestibular implant ideally would be implanted beneath the scalp, in a well countersunk in the skull posterior to the mastoid cavity. To avoid skin breakdown and poor cosmesis, the hermetically packaged device should be no thicker than ~1 cm and should be continuously recharged via a transcutaneous inductive link. The thickness and power consumption of our present device are largely determined by the gyro sensors, which are 7 mm on edge and collectively account for up to 90% of the power use. Rotational sensors in smaller packages with lower power consumption, ideally packaged with 3 orthogonal sensors per device, would facilitate development of a vestibular prostheses optimized for human use.

Our findings regarding the 3D AVOR of normal chinchillas are consistent with prior studies of rodents and lagomorphs using 1D or 2D eye recording techniques.[59;53;64;46] The normal chinchilla 3D AVOR is (partially) compensatory over 0.1–10 Hz; approximately conjugate; similar in gain for yaw, LARP and RALP; and symmetric with respect to sense of rotation (to within ~10%). These results suggest that despite its lateral eye orientation, the chinchilla is an appropriate animal model for vestibular prosthesis research meant to lay a foundation for subsequent studies in humans.

Pulsatile stimuli as used here are exclusively excitatory. For a unilateral vestibular prosthesis to encode head movements in all directions (including those that normally *inhibit* canals of the implanted labyrinth), the central nervous system must adapt to a tonic rate of stimulation, about which varying pulse rates encode excitatory and inhibitory head rotations. Setting the resting rate above the typical resting rate of vestibular nerve afferents can expand the dynamic range for encoding inhibitory head rotations. Merfeld, Gong, Lewis and colleagues observed evidence of adaptation over hours to months in chronically stimulated animals, with an apparent training effect increasing the speed of adaptation to step changes in tonic stimulus rate.[65;

33;32] Combined with the rapid decrease of eye movement asymmetry we observed acutely in chinchillas, these findings suggest that a unilaterally implanted device should be sufficient to restore bidirectional vestibular sensation. This is of practical importance, because the cost and surgical risk of bilateral vestibular implantation would limit clinical utility.

Adding a 3-axis linear accelerometer to the device to measure linear acceleration would incur negligible additional volume and power consumption compared to the 3 existing gyros. However, we have so far constrained our focus to emulating the SCC's and AVOR, for two reasons. First, SCC sensation and the AVOR dominate gaze stabilization for most activities in which our vestibular-deficient patients complain of visual disturbance, because retinal image slip due to angular motion of the eyes and head dominate slip due to translation when one is fixating a target greater than ~1m away. Second, whereas every afferent neuron in a given SCC's ampullary nerve encodes head rotation with the same axis and direction, the macular nerves innervating the utricle and saccule each contain afferents with a broad range of directional sensitivities, making selective emulation of normal utricular and saccular function much harder to achieve with electrodes of limited spatial density and selectivity.[36;39;40; 37;38]

While assaying cochlear function was outside the scope of the present phase of this research, maintaining hearing will be an important aim in clinical application of a vestibular prosthesis. One approach to test this in our experimental animals would be to use auditory-evoked brainstem responses to assay cochlear function before and after vestibular implantation.

Acknowledgments

We gratefully acknowledge: Todd Whitehurst, Tom Mehl and Cliff Brainard (Advanced Bionics Corporation), who helped with current source design, board layout and fabrication, respectively; Hamish MacDougall (Sydney University), who helped create the VOG system used in this work; Patpong Jiradejvong, Dale Roberts, Paul Gilka and Adrian Lasker (Johns Hopkins), who provided technical assistance with scleral coil recording and soldering; Russell Hayden and Thuy Melvin (Johns Hopkins), who assisted in some of the experiments; Daniel Merfeld (Jenks Vestibular Laboratory, Massachusetts Eye & Ear Infirmary), whose advice has helped foster this work; and Lloyd Minor (Johns Hopkins Otolaryngology – Head & Neck Surgery), whose mentorship has been integral to the success of this research. This work was supported by the National Institute on Deafness and Other Communication Disorders (K08-DC006216 and R01-DC002390) and by an American Otological Society Clinician-Scientist Award and a Johns Hopkins School of Medicine Ross Clinician-Scientist Award to CCDS.

References

1. Carey, JP.; Della Santina, CC. Principles of applied vestibular physiology. In: Cummings, CW.; Haughey, BH.; Thomas, JR.; Harker, LA.; Flint, PW.; Robbins, KT.; Schuller, DE.; Richardson, MA., editors. Cummings Otolaryngology - Head & Neck Surgery. Vol. 4. Philadelphia: Elsevier Mosby; 2005. p. 3115-3159.
2. Grossman GE, Leigh RJ, Bruce EN, Huebner WP, Lanska DJ. Performance of the human vestibuloocular reflex during locomotion. J Neurophysiol July;1989 62(1):264–272. [PubMed: 2754477]
3. Grossman GE, Leigh RJ. Instability of gaze during locomotion in patients with deficient vestibular function. Ann Neurol May;1990 27(5):528–532. [PubMed: 2360793]
4. Goldberg JM. The vestibular end organs: morphological and physiological diversity of afferents. Curr Opin Neurobiol Aug;1991 1(2):229–235. [PubMed: 1821186]
5. Della Santina CC, Potyagaylo V, Migliaccio AA, Minor LB, Carey JP. Orientation of human semicircular canals measured by three-dimensional multiplanar CT reconstruction. J Assoc Res Otolaryngol Sept;2005 6(3):191–206. [PubMed: 16088383]
6. Trillenberg P, Shelhamer M, Roberts DC, Zee DS. Cross-axis adaptation of torsional components in the yaw-axis vestibulo-ocular reflex. Exp Brain Res Jan;2003 148(2):158–165. [PubMed: 12520403]
7. Robinson DA. Plasticity in the oculomotor system. Fed Proc Apr;1982 41(6):2153–2155. [PubMed: 7075788]

8. Leigh, RJ.; Zee, DS. The Neurology of Eye Movements. Vol. 3. New York: Oxford Univ. Press; 1999.
9. Grossman GE, Leigh RJ, Abel LA, Lanska DJ, Thurston SE. Frequency and velocity of rotational head perturbations during locomotion. Exp Brain Res 1988;70(3):470–476. [PubMed: 3384048]
10. Tabak S, Collewijn H, Boumans LJ, van der SJ. Gain and delay of human vestibulo-ocular reflexes to oscillation and steps of the head by a reactive torque helmet. I. Normal subjects. Acta Otolaryngol Nov;1997 117(6):785–795. [PubMed: 9442816]
11. Collewijn H, Smeets JB. Early components of the human vestibulo-ocular response to head rotation: latency and gain. J Neurophysiol July;2000 84(1):376–389. [PubMed: 10899212]
12. Yasui S, Young LR. On the predictive control of foveal eye tracking and slow phases of optokinetic and vestibular nystagmus. J Physiol Feb;1984 347:17–33. [PubMed: 6707954]
13. Crane BT, Demer JL. Human horizontal vestibulo-ocular reflex initiation: effects of acceleration, target distance, and unilateral deafferentation. J Neurophysiol Sept;1998 80(3):1151–1166. [PubMed: 9744929]
14. Gillespie MB, Minor LB. Prognosis in bilateral vestibular hypofunction. Laryngoscope Jan;1999 109 (1):35–41. [PubMed: 9917037]
15. Grunbauer WM, Dieterich M, Brandt T. Bilateral vestibular failure impairs visual motion perception even with the head still. Neuroreport June;1998 9(8):1807–1810. [PubMed: 9665605]
16. Minor LB. Gentamicin-induced bilateral vestibular hypofunction. JAMA Feb;1998 279(7):541–544. [PubMed: 9480366]
17. Cohen B, Suzuki JI, Bender MB. Eye movements from semicircular canal nerve stimulation in the cat. Ann Otol Rhinol Laryngol Mar;1964 73:153–169. [PubMed: 14128701]
18. Cohen B, Suzuki JI, SHANZER S. An analysis of ocular nystagmus induced by semicircular canal nerve stimulation. Trans Am Neurol Assoc 1963;88:200–201. [PubMed: 14272222]
19. Suzuki JI, Goto K, Tokumasu K, Cohen B. Implantation of electrodes near individual vestibular nerve branches in mammals. Ann Otol Rhinol Laryngol Aug;1969 78(4):815–826. [PubMed: 4979119]
20. Suzuki JI, Cohen B. Head, eye, body and limb movements from semicircular canal nerves. Exp Neurol Nov;1964 10:393–405. [PubMed: 14228399]
21. Suzuki JI, Cohen B, Bender MB. Compensatory eye movements induced by vertical semicircular canal stimulation. Exp Neurol Feb;1964 9:137–160. [PubMed: 14126123]
22. Fluur E. Influences of semicircular ducts on extraocular muscles. Acta Otolaryngol Suppl 1959;149:1–46. [PubMed: 13660800]
23. Szentagothai J. The elementary vestibulo-ocular reflex arc. J Neurophysiol Nov;1950 13(6):395–407. [PubMed: 14784863]
24. Ewald, JR. Physiologische untersuchugen uber das Endorgans des Nervus Octavus. Wiesbaden: Bergmann; 1892.
25. Goldberg JM, Smith CE, Fernandez C. Relation between discharge regularity and responses to externally applied galvanic currents in vestibular nerve afferents of the squirrel monkey. J Neurophysiol June;1984 51(6):1236–1256. [PubMed: 6737029]
26. Ezure K, Cohen MS, Wilson VJ. Response of cat semicircular canal afferents to sinusoidal polarizing currents: implications for input-output properties of second-order neurons. J Neurophysiol Mar;1983 49(3):639–648. [PubMed: 6834091]
27. Minor LB, Goldberg JM. Vestibular-nerve inputs to the vestibulo-ocular reflex: a functional-ablation study in the squirrel monkey. J Neurosci June;1991 11(6):1636–1648. [PubMed: 2045879]
28. Zeng, F-G.; Popper, AN.; Fay, RR. Cochlear Implants: Auditory Prostheses and Electric Hearing. New York: Springer-Verlag; 2004.
29. Clark, G. Cochlear Implants: Fundamentals and Applications. New York: Springer; 2003.
30. Gong W, Merfeld DM. System design and performance of a unilateral horizontal semicircular canal prosthesis. IEEE Trans Biomed Eng Feb;2002 49(2):175–181. [PubMed: 12066886]
31. Gong W, Merfeld DM. Prototype neural semicircular canal prosthesis using patterned electrical stimulation. Ann Biomed Eng May;2000 28(5):572–581. [PubMed: 10925955]
32. Merfeld DM, Gong W, Morrissey J, Saginaw M, Haburcakova C, Lewis RF. Acclimation to chronic constant-rate peripheral stimulation provided by a vestibular prosthesis. IEEE Trans Biomed Eng Nov;2006 53(11):2362–2372. [PubMed: 17073343]

33. Lewis RF, Gong W, Ramsey M, Minor L, Boyle R, Merfeld DM. Vestibular adaptation studied with a prosthetic semicircular canal. J Vestib Res 2002;12(2–3):87–94. [PubMed: 12867667]
34. Wang H, Merchant SN, Sorensen MS. A Downloadable Three-Dimensional Virtual Model of the Visible Ear. ORL J Otorhinolaryngol Relat Spec Nov;2006 69(2):63–67. [PubMed: 17124433]
35. Curthoys IS, Oman CM. Dimensions of the horizontal semicircular duct, ampulla and utricle in rat and guinea pig. Acta Otolaryngol Jan;1986 101(1–2):1–10. [PubMed: 3515839]
36. Curthoys IS. Eye movements produced by utricular and saccular stimulation. Aviat Space Environ Med Sept;1987 58(9 Pt 2):A192–A197. [PubMed: 3675491]
37. Fluur E, Mellstrom A. The otolith organs and their influence on oculomotor movements. Exp Neurol Jan;1971 30(1):139–147. [PubMed: 5542195]
38. Fluur E, Mellstrom A. Saccular stimulation and oculomotor reactions. Laryngoscope Nov;1970 80 (11):1713–1721. [PubMed: 5481001]
39. Goto F, Meng H, Bai R, Sato H, Imagawa M, Sasaki M, Uchino Y. Eye movements evoked by the selective stimulation of the utricular nerve in cats. Auris Nasus Larynx Dec;2003 30(4):341–348. [PubMed: 14656558]
40. Goto F, Meng H, Bai R, Sato H, Imagawa M, Sasaki M, Uchino Y. Eye movements evoked by selective saccular nerve stimulation in cats. Auris Nasus Larynx Sept;2004 31(3):220–225. [PubMed: 15364355]
41. Della Santina CC. Unpublished measurements on semicircular canal plane orientations in chinchillas. 2004
42. Hullar TE, Williams CD. Geometry of the semicircular canals of the chinchilla (Chinchilla laniger). Hear Res Mar;2006 213(1–2):17–24. [PubMed: 16439079]
43. Hirvonen TP, Minor LB, Hullar TE, Carey JP. Effects of intratympanic gentamicin on vestibular afferents and hair cells in the chinchilla. J Neurophysiol Feb;2005 93(2):643–655. [PubMed: 15456806]
44. Della Santina, CC.; Migliaccio, AA.; Park, HJ.; Anderson, ICW.; Jiradejvong, P.; Minor, LB.; Carey, JP. 3D Vestibuloocular reflex, afferent responses and crista histology in chinchillas after unilateral intratympanic gentamicin. Assoc. for Research in Otolaryngology Annual Mtg.; 2005; New Orleans. 2005.
45. Carey JP, Minor LB, Peng GC, Della Santina CC, Cremer PD, Haslwanter T. Changes in the three-dimensional angular vestibulo-ocular reflex following intratympanic gentamicin for Meniere's disease. J Assoc Res Otolaryngol Dec;2002 3(4):430–443. [PubMed: 12486598]
46. Jones GE, Balaban CD, Jackson RL, Wood KA, Kopke RD. Effect of trans-bullar gentamicin treatment on guinea pig angular and linear vestibulo-ocular reflexes. Exp Brain Res Oct;2003 152 (3):293–306. [PubMed: 12898099]
47. Robinson DA. A method of measuring eye movement using a scleral search coil in a magnetic field. IEEE Trans Biomed Eng Oct;1963 10:137–145. [PubMed: 14121113]
48. Migliaccio AA, MacDougall HG, Minor LB, Della Santina CC. Inexpensive system for real-time 3-dimensional video-oculography using a fluorescent marker array. J Neurosci Methods Apr;2005 143 (2):141–150. [PubMed: 15814146]
49. Migliaccio AA, Schubert MC, Jiradejvong P, Lasker DM, Clendaniel RA, Minor LB. The three-dimensional vestibulo-ocular reflex evoked by high-acceleration rotations in the squirrel monkey. Exp Brain Res Dec;2004 159(4):433–446. [PubMed: 15349709]
50. Migliaccio AA, Todd MJ. Real-time rotation vectors. Australas Phys Eng Sci Med June;1999 22(2): 73–80. [PubMed: 10474978]
51. Haslwanter T. Mathematics of three-dimensional eye rotations. Vision Res June;1995 35(12):1727–1739. [PubMed: 7660581]
52. Hess BJ, Dieringer N. Spatial organization of linear vestibuloocular reflexes of the rat: responses during horizontal and vertical linear acceleration. J Neurophysiol Dec;1991 66(6):1805–1818. [PubMed: 1812218]
53. Gilchrist DP, Curthoys IS, Cartwright AD, Burgess AM, Topple AN, Halmagyi M. High acceleration impulsive rotations reveal severe long-term deficits of the horizontal vestibulo-ocular reflex in the guinea pig. Exp Brain Res Dec;1998 123(3):242–254. [PubMed: 9860262]

54. Straumann D, Zee DS. Three-dimensional aspects of eye movements. Curr Opin Neurol Feb;1995 8 (1):69–71. [PubMed: 7749520]
55. Abbas, PJ.; Miller, CA. Biophysics and Physiology. In: Zeng, F-G.; Popper, AN.; Fay, RR., editors. Cochlear Implants: Auditory Prostheses and Electric Hearing. New York: Springer-Verlag; 2004. p. 149-212.
56. Neural Prostheses. Englewood Cliffs, NJ: Prentice-Hall; 1990.
57. Macherey O, van Wieringen A, Carlyon RP, Deeks JM, Wouters J. Asymmetric pulses in cochlear implants: effects of pulse shape, polarity, and rate. J Assoc Res Otolaryngol Sept;2006 7(3):253–266. [PubMed: 16715356]
58. Baird RA, Desmadryl G, Fernandez C, Goldberg JM. The vestibular nerve of the chinchilla. II. Relation between afferent response properties and peripheral innervation patterns in the semicircular canals. J Neurophysiol July;1988 60(1):182–203. [PubMed: 3404216]
59. Merwin WH Jr, Wall C III, Tomko DL. The chinchilla's vestibulo-ocular reflex. Acta Otolaryngol Sept;1989 108(3–4):161–167. [PubMed: 2816332]
60. Hullar TE, Della Santina CC, Hirvonen T, Lasker DM, Carey JP, Minor LB. Responses of irregularly discharging chinchilla semicircular canal vestibular-nerve afferents during high-frequency head rotations. J Neurophysiol May;2005 93(5):2777–2786. [PubMed: 15601735]
61. Goldberg JM, Desmadryl G, Baird RA, Fernandez C. The vestibular nerve of the chinchilla. V. Relation between afferent discharge properties and peripheral innervation patterns in the utricular macula. J Neurophysiol Apr;1990 63(4):791–804. [PubMed: 2341877]
62. Loeb GE, Peck RA, Smith DW. Microminiature molding techniques for cochlear electrode arrays. J Neurosci Methods Dec;1995 63(1–2):85–92. [PubMed: 8788052]
63. Bierer, J., Bonham, B., Rebscher, S., and Snyder, R. The neurophysiological effects of simulated auditory prosthesis stimulation. 1st QPR, Neural Prosthesis Program Contract N01-DC-02-1006. 12–31–2002. National Institutes of Health.
64. Baarsma EA, Collewijn H. Changes in compensatory eye movements after unilateral labyrinthectomy in the rabbit. Arch Otorhinolaryngol Dec;1975 211(4):219–230. [PubMed: 1243643]
65. Lewis RF, Haburcakova C, Merfeld DM. Tilt psychophysics measured in nonhuman primates. Ann N Y Acad Sci Apr;2005 1039:294–305. [PubMed: 15826983]

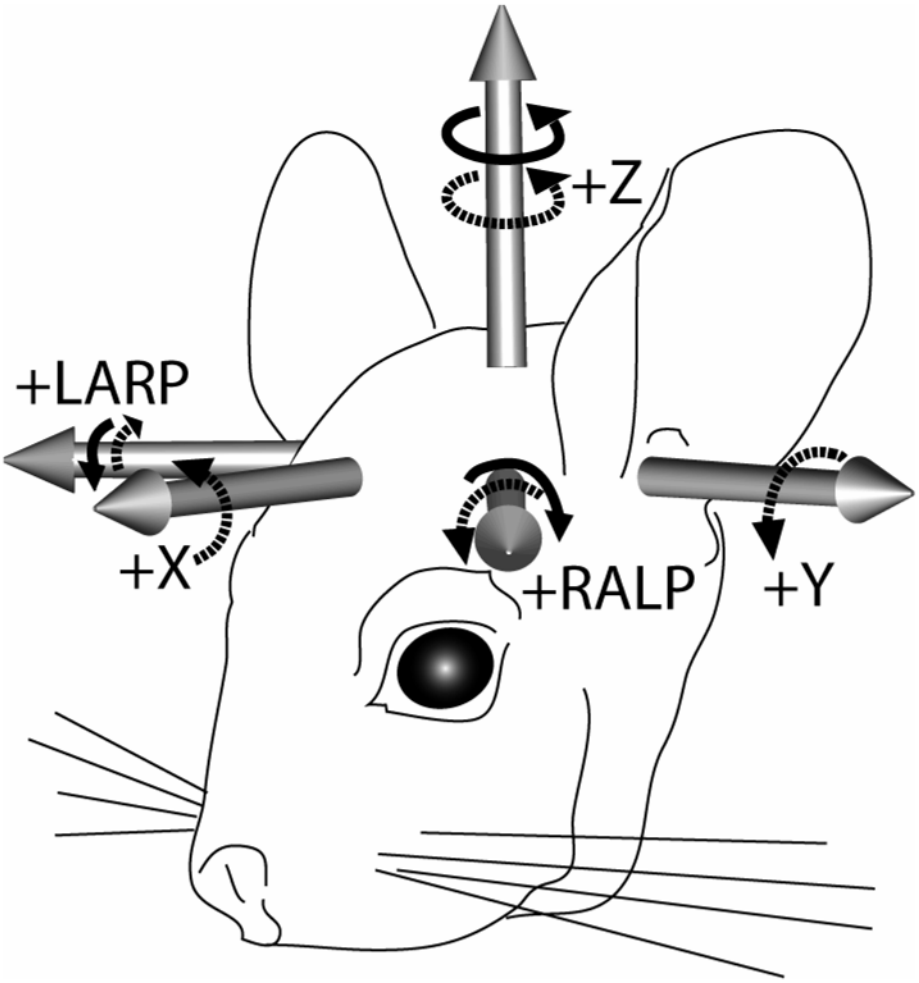

Figure 1.

Head coordinate system used for head and eye rotation data. When the animal is positioned in a holder that pitches the occlusal plane 50° nose down, the Z plane (approximating the horizontal SCCs) is Earth-horizontal, the Y (pitch) plane is midsagittal, the X (roll) plane is perpendicular to the Y and Z planes, the intersection of the X and Z planes is along the interaural axis, and the origin of the coordinate system is centered on the Earth-vertical axis of the motor that rotates the animal. The X, Y and Z axis positive tips are anterior, left and superior, respectively. We approximated the positive left-anterior/right-posterior (LARP) axis normal to the LARP plane as (X,Y,Z)=(1,−1,0), and the right-anterior/left-posterior (RALP) axis as (X,Y,Z)=(1,1,0). Right-hand-rule rotations about an axis' positive tip (dashed arrows) are positive polarity. Solid arrows show sense of head rotations that *excite* the left labyrinth's SCCs while *inhibiting* the coplanar right SCCs.

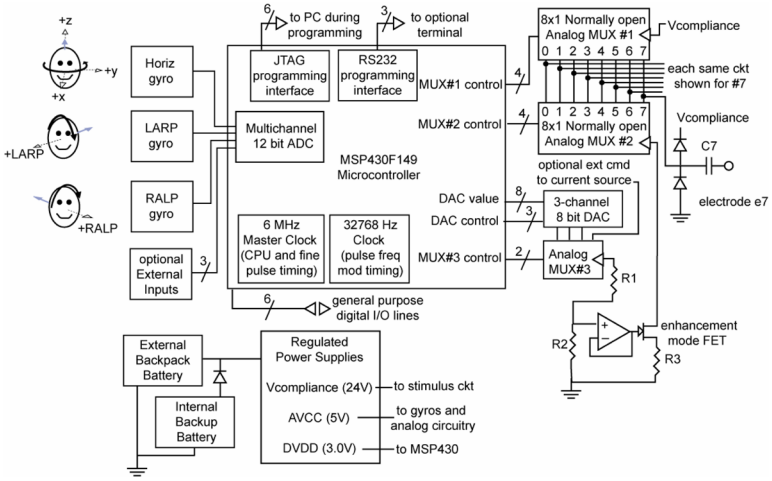

Figure 2.

Conceptual diagram of prosthesis circuitry. Three mutually orthogonal gyro sensors aligned with the horizontal, anterior and posterior semicircular canals of the left labyrinth measure head rotation about the head axes shown (dashed lines with open arrows). Head rotation in the sense shown by black arrows “excites” a higher pulse rate on the corresponding gyro’s channel. Gyro signals are digitized within the MSP430 microcontroller’s analog-digital converter module, then optionally filtered and/or transformed via a coordinate system rotation to account for misalignment of gyros with SCCs. Resulting signals set the frequency modulation of biphasic pulses according to a sigmoid operating curve (Figure 3). A 3-channel digital-analog converter sets command current for a shared current source, which switches between pairs of electrodes to generate the cathodic phase of a pulse and then a charge-recovery anodic phase with oppositely directly current through the same electrode pair. All parameters may be set through a JTAG programming interface or RS-232 serial interface with the device *in situ*.

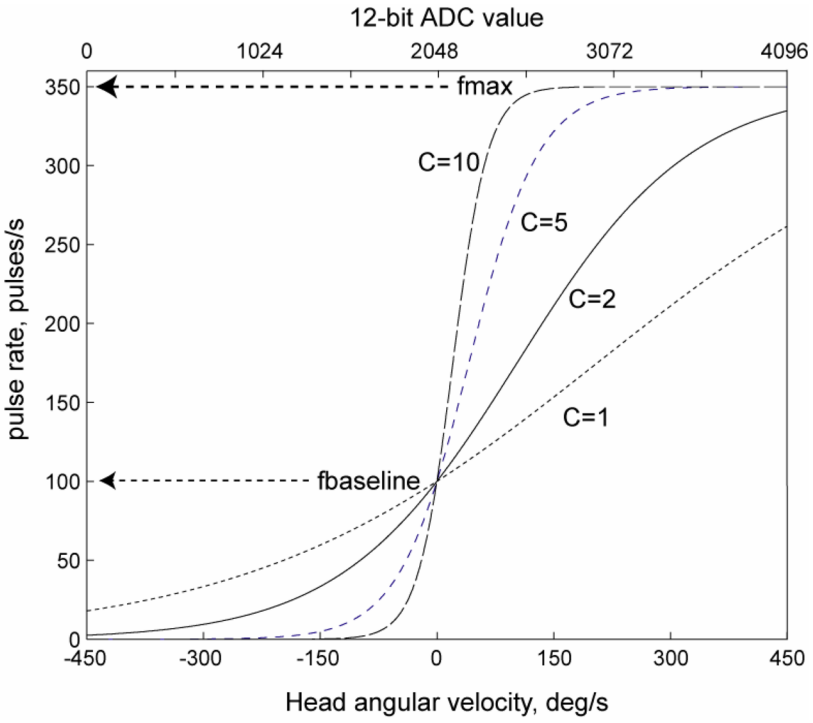

Figure 3.
Prosthesis pulse rate versus head velocity operating characteristic curves defined by Equation 1 with resting rate 100 pulse/s, max rate 350 pulse/s, and compression factor C of 1, 2, 5, or 10.

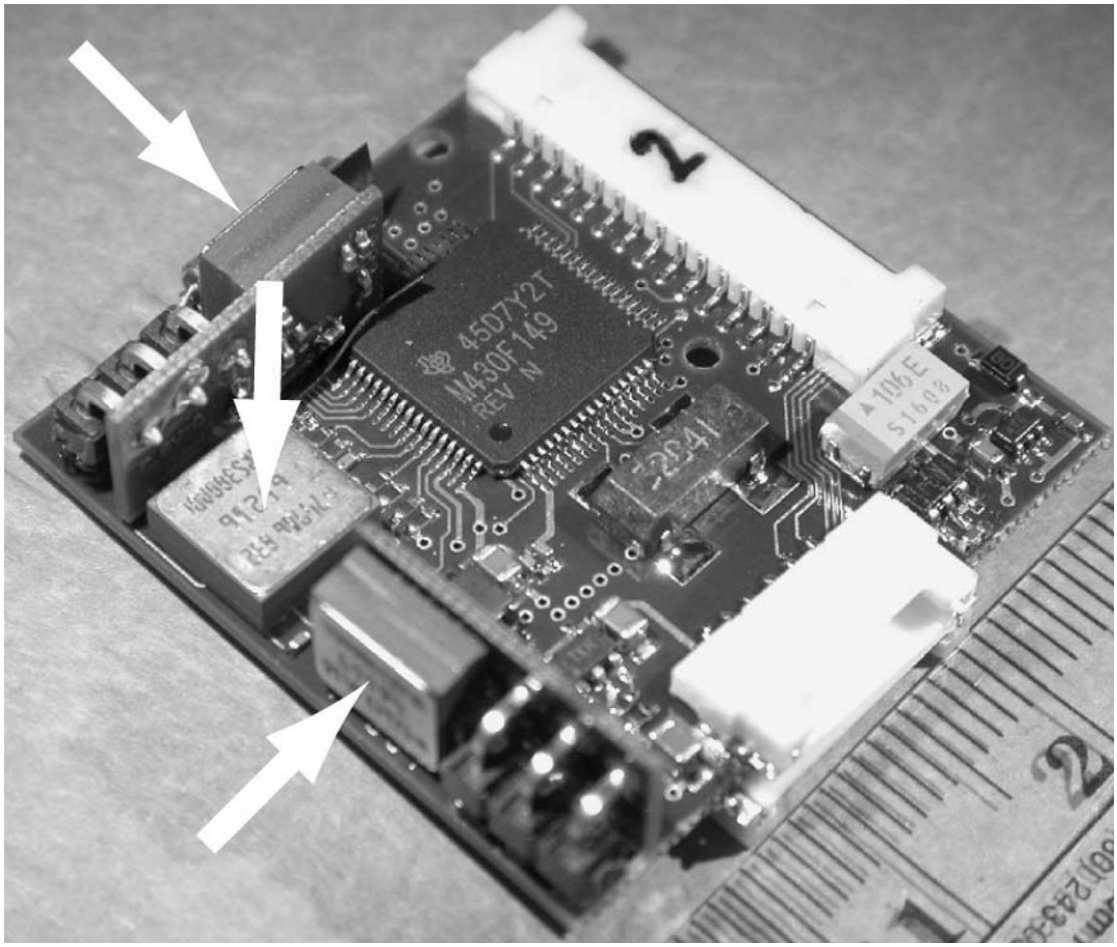

Figure 4.
Prosthesis circuitry. Arrows = gyro rate sensors, two of which are on boards perpendicular to the mother board. Scale = cm.

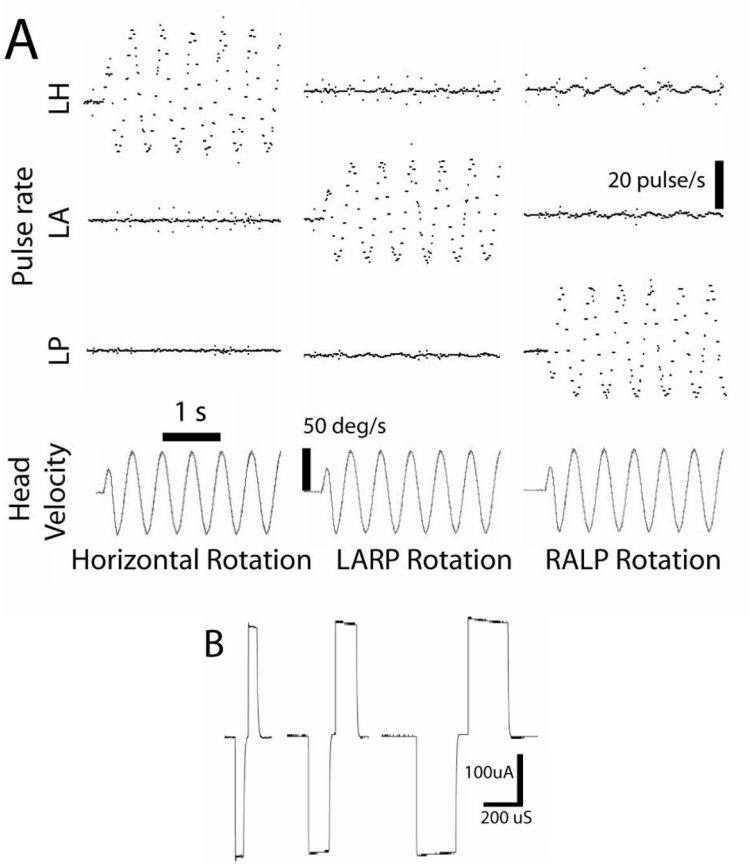

Figure 5.

(A) Pulse rates on each of 3 electrode channels (LH = left horizontal SCC, LA = left anterior, LP = left posterior) encoding components of 3 different 2 Hz, 50 deg/s rotations of the device on the animal's head about each axis. **(B)** Biphasic stimulus current delivered via one pair of the electrodes immersed in 0.9% NaCl during 240 μA/phase pulses of 50, 120 and 200 μs/phase, with cathodic-to-anodic intrapulse interval set to 10% of the duration of each phase.

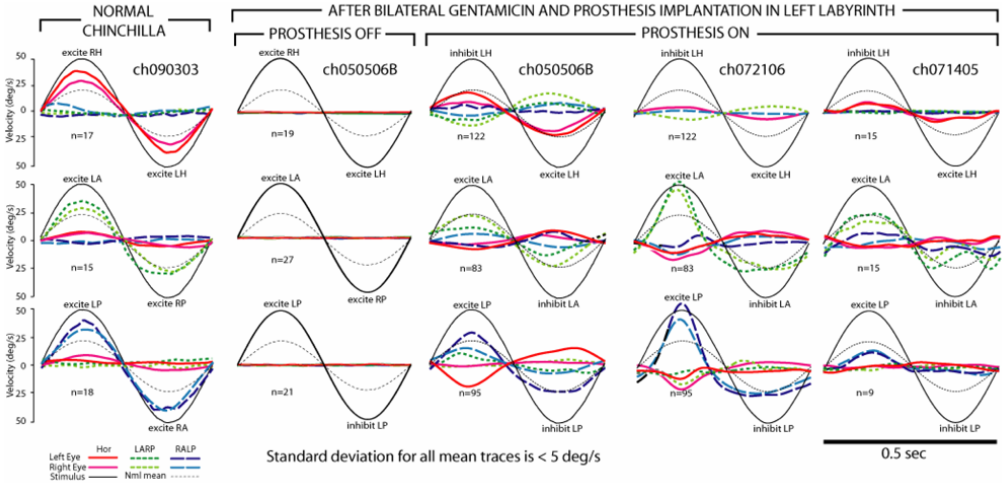

Figure 6.

(Column 1) Mean head rotation and eye rotations of a normal chinchilla (ch090303) during 2 Hz, 50°/s head rotations without vision, in horizontal (top), LARP (middle) and RALP (bottom) planes. This animal's gains were higher than average. For all panels, a sinusoid indicating the grand mean response of all 5 normal animals to 2 Hz, 50°/s head rotation in the appropriate plane (thin dotted line) is shown for comparison; number of cycles pooled is listed; standard deviation of each trace at each time point is < 5°/s, head or eye traces are inverted as required to facilitate visual comparison; the sense of head rotation is listed in each panel. **(Column 2)** Responses under same testing conditions for chinchilla treated bilaterally with gentamicin and then implanted with electrodes in the 3 left SCC's (ch050506B), with prosthetic stimulation off. **(Column 3)** Responses of ch050506B to same head rotations, 3.5 hrs after activation of the multichannel prosthesis (parameters in text). **(Column 4)** Responses of ch072106 5 days hrs after activation. **(Column 5)** Responses of ch071405 3 days hrs after activation.

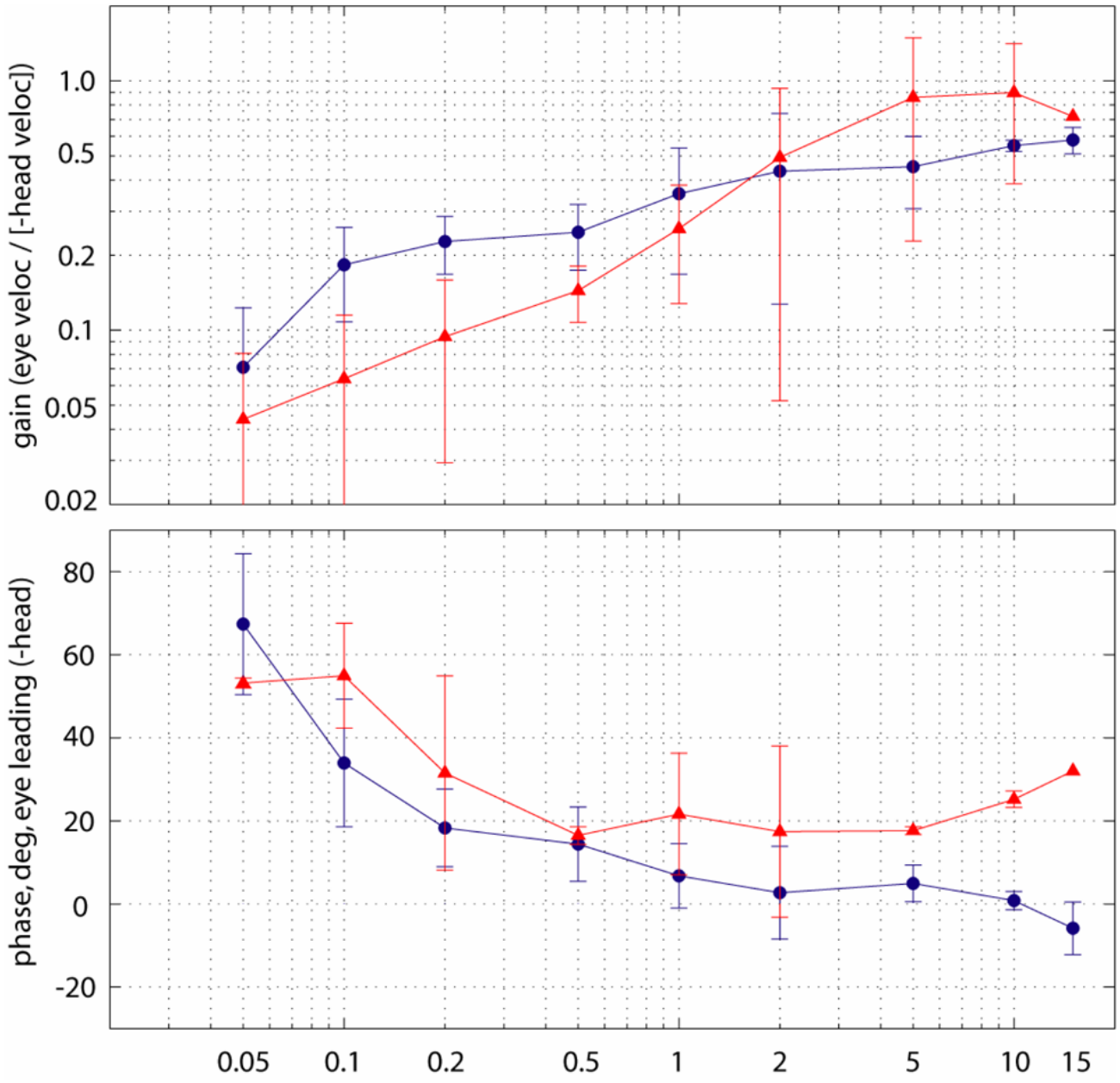

Figure 7.

Mean gain (top) and phase lead (bottom) of eye versus the ideal response (−1 × head velocity) for the horizontal component of 3D angular AVOR for 5 normal chinchillas during 50°/s peak horizontal passive head rotation in darkness (circles) and for 3 bilaterally gentamicin-treated chinchillas during prosthetic stimulation encoding 50°/s horizontal passive head rotations (triangles). Error bars denote ±1SD. Only 1 animal yielded data for electrical stimulation at 15 Hz. The prosthetic stimulation responses have a shallower slope of gain versus frequency (nearly 0.5 on a log-log plot) and an upward shift in phase lead compared to normal. Gains for bilaterally-gentamicin-treated animals without prosthetic stimulation were below the physiologic and measurement noise of the recording system.

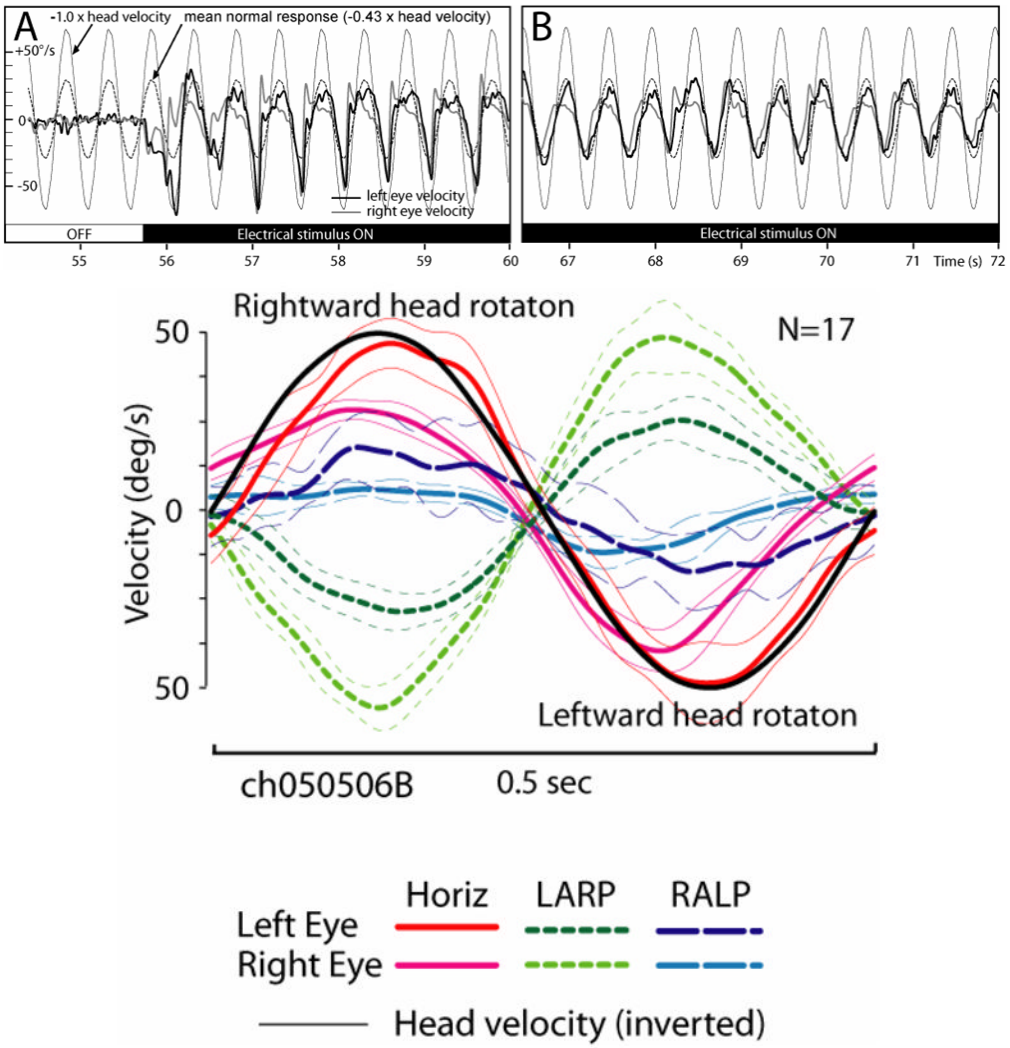

Figure 8.

(A & B) Horizontal components of left and right eye rotational velocity for the same chinchilla as Figure 1, Columns 2 and 3 (ch050506B), during 2Hz 50°/s peak sinusoidal horizontal head rotations without (**A**, t<55.7 sec) and then with (**A**, t>55.7 sec) prosthetic electrical stimulation pulse-frequency-modulated by horizontal head velocity. Only the left horizontal SCC electrodes were activated. Stimulus parameters: cathodic-first biphasic pulses, bipolar electrode pair in the left horizontal SCC ampulla, 150 μA/phase, 200 μs/phase, f_{peak} 300 pulse/s, $f_{baseline}$ 100, C=5. Head rotation without electrical stimulation elicited no AVOR. Onset of electrical stimulation produced brisk, asymmetric horizontal nystagmus. **(B)** Slow phase nystagmus is already more symmetric in direction <20 sec after onset, tracking horizontal head velocity with a mean gain for the each eye similar to the mean response for normal animals (dashed gray line). **(C)** Mean±1SD cycle-by-cycle average for horizontal, LARP and RALP components for both eyes over the 17 cycles beginning at t=67 of the trial shown in A & B.

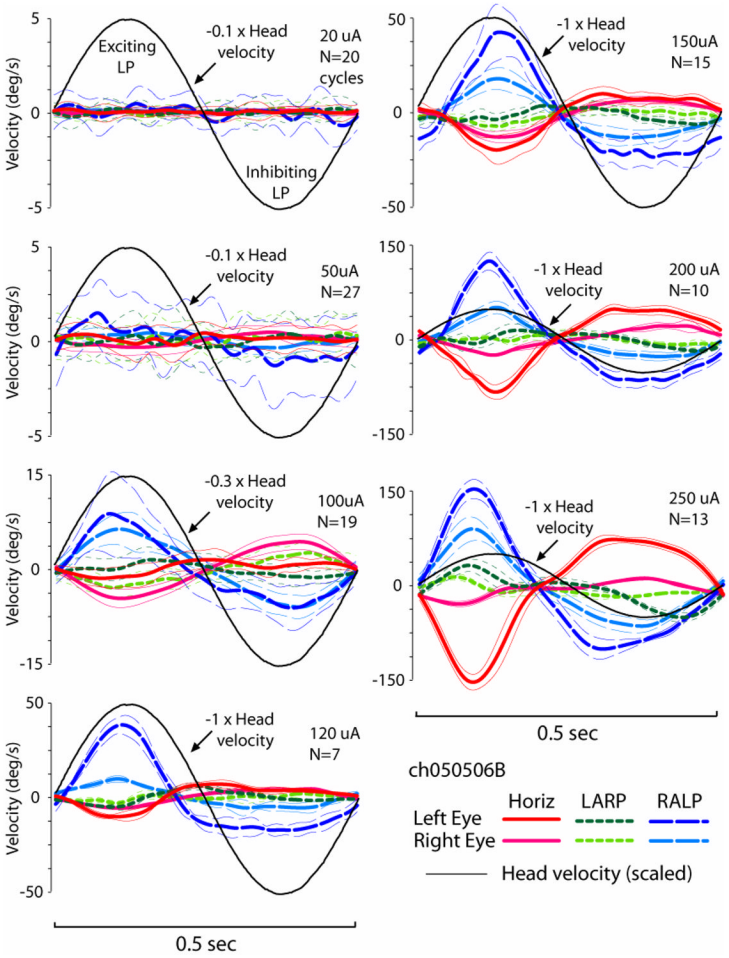

Figure 9.

AVOR responses during a 2 Hz, 50°/s RALP head rotation of ch050506B encoded by prosthetic stimulation delivered by a monopolar electrode in the LP SCC ampulla with respect to a distant reference. For each panel, stimulus current is labeled; all other parameters were kept constant ($f_{baseline}$ 100, f_{peak} 350, C=5, 200 us/phase, cathodic first). In each, the ordinate axis and inverted head velocity trace have been scaled to enhance visibility all components of the response. Barely visible at 50 μA, the response at 100 μA includes conjugate RALP rotations similar to normal chinchilla responses, except for a horizontal component that could indicate horizontal SCC ampulla or otolith nerve stimulation. At 250 μA, the LP response has grown to over 150°/s peak velocity, but the spurious horizontal component nearly equals it.